Rev. Adv. Mater. Sci. 35 (2013) 25-38

STRESS-DRIVEN ROTATIONS OF HIGH-ANGLE GRAIN BOUNDARIES IN NANOCRYSTALLINE MATERIALS

S.V. Bobylev[1,2] and I.A. Ovid'ko[1,2,3]

[1]Department of Mathematics and Mechanics, St. Petersburg State University, Universitetskii pr. 28, Staryi Peterhof, St. Petersburg 198504, Russia
[2]Institute of Problems of Mechanical Engineering, Russian Academy of Sciences, Bolshoj 61, Vasil. Ostrov, St. Petersburg 199178, Russia
[3]St. Petersburg State Polytechnical University, St. Petersburg 195251, Russia

Received: October 10, 2013

Abstract. A new mechanism/mode of plastic deformation occurring through stress-driven rotations of high-angle grain boundaries (GBs) in subsurface areas of nanocrystalline materials is theoretically described. It is demonstrated that a rotation of a high-angle GB produces nanoscale plastic flow and leads to formation of a disclination (rotational defect) whose strength and energy depend on both GB parameters (misorientation angle, etc.) and rotation angle. The suggested approach serves as a generalization of the theoretical model [Bobylev and Ovid'ko, Phys. Rev. Lett. **109**, 175501 (2012)] describing stress-driven rotations of low-angle tilt boundaries composed of lattice dislocations in crystals. In the exemplary case of nickel, it is found that the rotations of high-angle GBs are energetically favorable processes in wide range of GB parameters. Each energetically favorable GB rotation is specified by its equilibrium rotation angle φ_{eq} associated with the energy minimum. Dependences of φ_{eq} on applied stress, GB misorientation and other geometric characteristics of a rotating GB are calculated which show the trends in realization of stress-driven rotations of high-angle GBs in deformed nanocrystalline solids. Our theory is consistent with the corresponding experimental data reported in the literature.

1. INTRODUCTION

Nanoscale deformation processes occurring in nanowires, micropillars and bulk nanocrystalline solids represents the subject of intensive research efforts motivated by both a wide range of their applications and large fundamental interest to specific deformation mechanisms/modes operating on the nanoscale level; see, e.g., [1-–25]. For instance, conventional lattice dislocation slip (which dominates in coarse-grained polycrystals) shows some unusual peculiarities in bulk nanocrystalline solids due to the combined *nanoscale and grain-boundary effects*, and, in addition, specific deformation mechanisms effectively come into play [1–3,6,7,10–15,21–24]. These mechanisms are GB sliding, rotational deformation, nanoscale twin deformation, stress-driven GB migration, and GB diffusional creep. In single crystalline nanowires and micropillars, the combined *nanoscale and free-surface effects* strongly influence plastic deformation. In particular, they lead to both lattice dislocation starvation [5] and operation of specific physical mechanisms of plastic flow, the namely nanoscale twin deformation, lattice slip controlled by surface dislocation sources, multiplane nanoscale shear, nanodisturbance deformation mode, plastic deformation carried by amorphization, etc. [5,8,9,13,16–20,25].

Recently a particular attention has been paid to nanowires and micropillars with nanocrystalline

Corresponding author: I.A. Ovidko, e-mail: ovidko@nano.ipme.ru

structures as solids where the three effects cooperatively operate which are the *nanoscale, grain-boundary and free-surface effects* [26–31]. The research in this area opens a rather unique opportunity to identify fundamental deformation mechanisms/modes simultaneously controlled by the three effects and thus understand physics of the mechanical properties exhibited by nanowires and micropillars with nanocrystalline structures. In particular, Jang and Greer [30] experimentally observed a new type of GB transformations – the namely GB rotations – in nanocrystalline Ni nanopillars under mechanical load. In Letter [32], GB rotations were theoretically described as stress-driven processes representing a new physical mechanism of plastic deformation in solids. Within the approach [32], stress-driven GB rotations effectively carry plastic flow in nanocrystalline nanowires, nanopillars and films as well subsurface areas of bulk nanocrystalline specimens due to the combined actions of the nanoscale, grain-boundary and free-surface effects.

In Letter [32], we theoretically described stress-driven rotations of low-angle tilt boundaries – GBs of the simplest geometric type - modeled as finite walls of lattice dislocations. At the same time, most nanocrystalline materials contain high-angle tilt GBs as dominating structural elements, while the fraction of low-angle GBs is comparatively small [33]. In general, physical properties and deformation behaviors of high-angle GBs can be significantly different from those of their low-angle counterparts [33–35]. For instance, in contrast to low-angle GBs, high-angle GBs effectively carry intergrain sliding and GB diffusional deformation modes capable of essentially contributing to plastic flow in solids with nanocrystalline structures [33–35]. In this context, it is very interesting to reveal the specific features of stress-driven rotations of high-angle GBs carrying plastic deformation in nanocrystalline nanowires, nanopillars and films as well as subsurface areas of bulk nanocrystalline specimens. (For shortness, hereinafter all these systems with nanocrystalline structures will be called nanocrystalline solids.) The main aim of this paper is to extend the approach [32] to the typical case of high-angle GBs and theoretically describe their stress-driven rotations carrying plastic deformation in nanocrystalline solids. In doing so, the structural geometry of high-angle GBs as well as the nanoscale, grain-boundary and free-surface effects cooperatively operating in nanocrystalline solids will be taken into consideration.

2. STRESS-DRIVEN ROTATIONS OF HIGH-ANGLE GRAIN BOUNDARIES IN NANOCRYSTALLINE SOLIDS: GENERAL ASPECTS AND GEOMETRY

Let us consider geometric features of plastic deformation mode occurring through stress-driven rotations of high-angle GBs in nanocrystalline solids. Fig. 1a schematically shows a two-dimensional section of a nanocrystalline solid consisting of nanoscale grains divided by GBs. The subsurface area of the solid contains a high-angle symmetric tilt boundary AB which is presented in the magnified inset in Fig. 1b. The GB plane makes the angle α with the specimen free surface and has the common point B with the free surface (Fig. 1b). Also, the GB AB forms the triple junction A with two static GBs AC and AD (Fig. 1b).

Within our model, we consider a rotation of the GB AB under the shear stress τ operating in the subsurface region of the mechanically loaded nanocrystalline specimen (Figs. 1b and 1c). In the initial state (Fig. 1b), the GB structures are geometrically balanced at the triple junction A distant by d from the free surface. It means that GBs AB, CA, and DA are specified by tilt misorientation angles providing no angle gap at the triple junction A which thereby does not create stresses in the initial state of the defect configuration (Fig. 1b). Rotations of the GB AB violate the geometric balance at the triple junction A which thereby becomes a stress source after the GB rotations; for details, see below.

Following the geometric theory of high-angle GBs in crystals [34], the GB AB can be effectively represented as a continuous homogeneous distribution of GB dislocations with infinitesimally small Burgers vectors. This representation (which generalizes the dislocation model of low-angle tilt boundaries as discrete distributions/walls of lattice dislocations with quantized Burgers vectors [34]) is well relevant for our further description of stress-driven rotations of high-angle GBs. The continuous dislocation distribution at the GB AB of finite extent is characterized by the sum (integral) Burgers vector $\mathbf{B}_0$ (Fig. 1b). In spirit of the geometric theory of GBs, its modulus B_0 is in the following Frank relationship [36] with the GB misorientation angle θ_0:

$$B_0 = 2l_0 \tan(\theta_0/2), \quad (1)$$

where l_0 denotes the initial length of the GB AB (Fig. 1b).

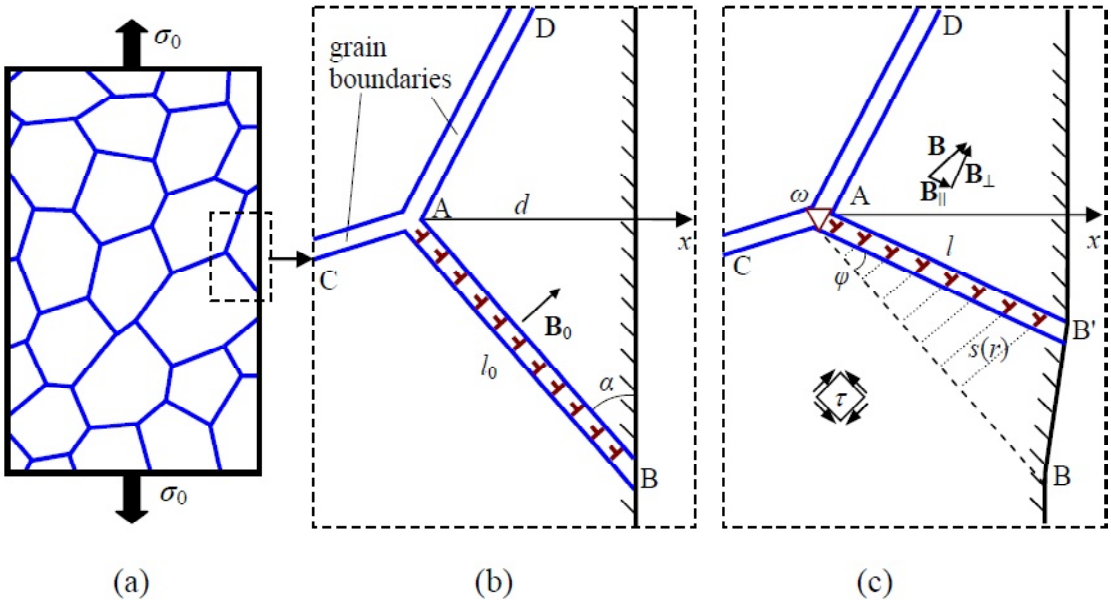

Fig. 1. (Color online) Stress-driven rotation of a high-angle grain boundary in a nanocrystalline solid near its free surface (a two-dimensional model). (a) Nanocrystalline specimen: general view. (b) and (c) show a magnified inset of the subsurface region where stress-driven rotation of tilt grain boundary occurs. (b) Initial state. High-angle grain boundary AB (entering the free surface at point B) is modeled as a continuous distribution of edge dislocations having infinitesimally small Burgers vectors. (c) Cooperative movement of grain boundary dislocations under the shear stress τ results in rotation of high-angle grain boundary (by angle φ) from its initial position AB to the final position AB'. During the rotation of the grain boundary, its part disappears at the free surface, and the corresponding free surface step BB' is formed.

Let us consider stress-driven rotation of the high-angle GB from its initial position AB (see dotted line in Fig. 1c) to a new position AB'. Within the representation of the GB AB as an ensemble of continuously distributed GB dislocations [34], the GB rotation (Fig. 1c) is associated with correlated movement of its GB dislocations and thereby carries plastic deformation (GB dislocation slip) under the shear stress τ. For definiteness, as with our previous model for rotation of low-angle tilt boundaries [32], the GB AB is assumed to be flat during the rotation process. That is, the stress-driven rotation of the high-angle GB (from its initial position AB to a new position AB') by angle φ occurs with the triple junction A playing the role of the rotation axis (Fig. 1c).

During the rotation of the GB, its structural geometry changes. In particular, in the case illustrated in Fig. 1c, a part of the rotating GB disappears at the free surface due to the GB rotation, and the corresponding free surface step BB' is formed. Also, by analogy with the case of low-angle tilt boundaries [32], the high-angle GB AB transforms from symmetric tilt boundary in the initial state (Fig. 1b) into asymmetric one in the final state after the rotation (Fig. 1c). It is related to the fact that the Burgers vectors of GB dislocations change their orientation relative to the GB plane during its rotation. As a result, for each GB dislocation, the Burgers vector component parallel to the GB plane appears, and the combined effects of these components provide the role of the asymmetric GB as a source of long-range stresses (Figs. 1c and 2). Besides, for each GB dislocation, the Burgers vector component normal to the GB plane decreases during the GB rotation (Figs. 1b, 1c, and 2). Since the normal component provides the tilt boundary misorientation [34], the rotation of the GB AB leads to a decrease in its misorientation ($\theta_0 \rightarrow \theta$, where $\theta < \theta_0$). In these circumstances, the balance of misorientation angles at the triple junction A is violated, and a non-zero angle gap ($\omega = \theta - \theta_0$) is generated at the triple junction A which thereby becomes a stress source. More precisely, in accordance with the theory of defects in solids, a GB junction with a non-zero angle gap represents a wedge disclination, a rotational defect serving as a powerful source of internal stresses [37,38]. So, as a consequence of the GB rotation (Figs. 1b and 1c), both the GB AB and the triple junction A be-

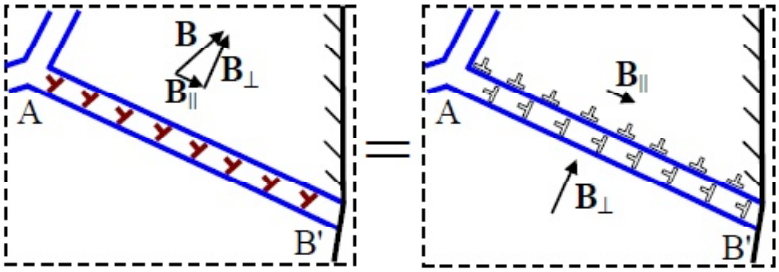

Fig. 2. (Color online) GB dislocation ensemble at the rotated GB (after its rotation to position AB') is represented as a superposition of the two continuous distributions of edge dislocations with Burgers vectors perpendicular and parallel to the GB plane. The first distribution is characterized by the sum Burgers vector $\mathbf{B}_{\perp}$ perpendicular to the GB plane. This GB dislocation distribution is associated with the symmetric tilt misorientation of the GB. The second distribution is characterized by the sum Burgers vector $\mathbf{B}_{\parallel}$ parallel to the GB plane. This GB dislocation distribution specifies asymmetry inherent to the rotated GB.

come stress sources whose elastic energies crucially contribute to the hampering force for the GB rotation process.

Now let us discuss general aspects of stress-driven GB rotations in nanocrystalline solids. As it has been noted in Introduction, the free-surface, nanoscale and grain-boundary effects strongly influence the GB rotation process. In particular, by analogy with low-angle tilt boundaries [32], there are the two free-surface effects enhancing the stress-driven rotation of high-angle GBs. First, for geometric reasons, the rotation process can diminish both the GB length and thereby its energy through disappearance of GB part(s) at the free surface (Figs. 1b and 1c). Second, the rotation-produced stresses of GBs and triple junctions (Fig. 1c) are effectively screened by the free surface, in which case GB rotations are favored in subsurface areas of solids (for details, see below).

The nanoscale and grain-boundary effects on the GB rotation manifest themselves, first of all, through suppression of conventional lattice dislocation slip in nanocrystalline solids. With these effects, GB processes – in particular, GB rotations - carrying plastic flow are initiated and enhanced in mechanically loaded nanocrystalline solids. Besides, GB rotations can intensively occur in namely nanocrystalline materials, because such materials contain extremely large amounts of GBs. Note that plastic deformation via GB rotations can occur in subsurface areas of coarse-grained polycrystals as well. However, with low amounts of GBs and dominant character of conventional lattice slip in polycrystals, stress-driven rotations of GBs hardly play a prominent role in plastic flow in polycrystals.

3. ENERGY CHARACTERISTICS OF STRESS-DRIVEN MIGRATION OF HIGH-ANGLE GRAIN BOUNDARIES IN NANOCRYSTALLINE SOLIDS

Let us calculate the equilibrium rotation angle of the GB AB (Fig. 1) as a function of various parameters characterizing the defect configuration under consideration. To do so, we should find the total energy change ΔW of the defect configuration during the GB rotation process. The energy change ΔW characterizing the GB rotation has the three terms:

$$\Delta W = W_1 - W_0 - A_{pl}, \qquad (2)$$

where W_0 and W_1 are the energies of the defect configuration in its initial and final states, respectively (Figs. 1b and 1c, respectively), and A_{pl} is the plastic flow work spent to the GB rotation under the shear stress τ. Hereinafter all the energies are written as those per unit length of the triple junction. That is, in our calculations of the energy characteristics, the three-dimensional picture is reduced to two-dimensional one (which nevertheless captures all essential physics of the GB rotation process).

As it has been noted previously, in the initial state (Fig. 1b), the angle gap is zero at the triple junction A which thereby does not create stresses. Therefore, the elastic energy of the defect configuration in its initial state (Fig. 1b) is taken as zero. Only the proper energy of the GB region contributes to W_0. As a result, we find

$$W_0 = \gamma_{GB}(\theta_0) l_0 = \gamma_{GB}(\theta_0) d / \sin\alpha, \qquad (3)$$

where $\gamma_{GB}(\theta)$ is the specific GB energy (per unit area of GB) sensitive to the misorientation angle θ_0 of the GB AB. The energies of the static GBs CA and

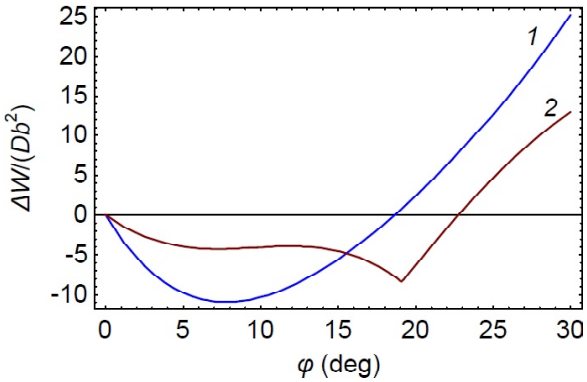

Fig. 3. (Color online) Dependences of the total energy change D*W* on the rotation angle j, for high-angle grain boundaries in nanocrystalline Ni. The dependences are calculated at $\tau = 0.06D$, $\alpha = 45°$, $\theta_0 = 15°$, $d = 100b$ (curve *1*) and $\tau = 0.08D$, $\alpha = 45°$, $\theta_0 = 20°$, $d = 50b$ (curve *2*).

DA (Fig. 1) are not taken into account in the energy change ΔW, because these GBs do not evolve during the rotation of the GB AB.

Let us consider the energy W_1 of the defect configuration in its final state (Fig. 1c) resulted from the GB rotation process. Note that the GB AB after the rotation is asymmetric. Therefore, its intrinsic ensemble of continuously distributed GB dislocations can be imaginarily divided into the two ones (Fig. 2). The first ensemble of GB dislocations with Burgers vectors normal to the GB plane provides the symmetric tilt GB misorientation. The second ensemble of GB dislocations with Burgers vectors parallel to the GB plane provides GB asymmetry and serves as a source of long-range stresses associated with this tilt asymmetry. In the circumstances under discussion, the energy W_1 is represented as the following sum:

$$W_1 = W^{\Delta} + W_{step} + W_p + \gamma_{GB}(\theta) l. \qquad (4)$$

Here W^{Δ} is the proper elastic energy of the wedge disclination A, W_p denotes the energy of stress fields created by continuously distributed GB dislocations with Burgers vectors parallel to the GB AB', W_{step} is the energy of the free surface step BB' (formed due to the rotation-induced enter of a part of the rotated GB on the free surface), and $l = d/\sin(\alpha + \varphi)$ is the length of the rotated GB in its position AB' (Fig. 1c).

Thus, with formulas (3) and (4), the total energy change ΔW is as follows:

$$\Delta W = W^{\Delta} + W_p + W_{step} + d\left[\gamma_{GB}(\theta)/\sin(\alpha+\varphi) - \gamma_{GB}(\theta_0)/\sin\alpha\right] - A_{pl}. \qquad (5)$$

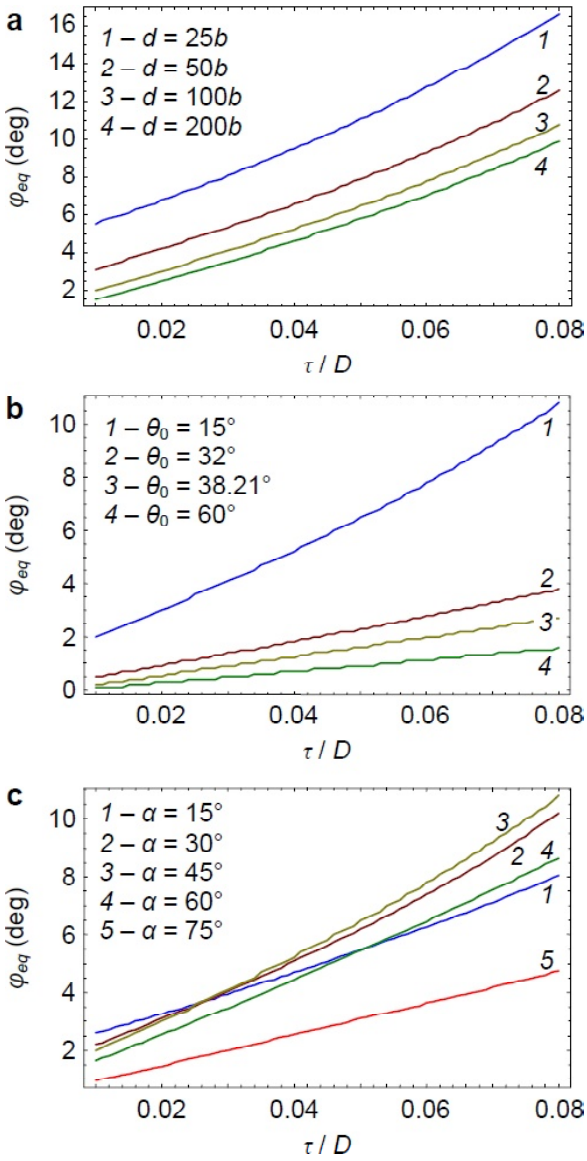

Fig. 4. (Color online) Dependences of the equilibrium rotation angle φ_{eq} on the applied shear stress τ at (a) $\theta_0 = 15°$, $\alpha = 45°$, and $d = 25b$, $50b$, $100b$, $200b$ (curves *1*, *2*, *3*, *4*, respectively); (b) $\alpha = 45°$, $d = 100b$, and $\theta_0 = 15°$, 32°, 38.21°, 60° (curves *1*, *2*, *3*, *4*, respectively); (c) $\theta_0 = 15°$, $d = 100b$, and $\alpha = 15°$, 30°, 45°, 60°, 75° (curves *1*, *2*, *3*, *4*, *5*, respectively).

The terms figuring on the right-hand side of formula (5) are calculated in Appendix. With these terms and formula (5), we calculated the total energy change ΔW in the experimentally examined [30] case of Ni. In doing so, we used the following values of parameters [39]: $G = 73$ GPa, $\nu = 0.34$, $b = 0.25$ nm, and $\gamma_s = 2.28$ J/m^2. Also, value of the GB energy density is chosen as $\gamma_s = 1.5$ J/m^2.

Fig. 3 presents typical dependences of ΔW on the GB rotation angle φ. In particular, curve 1 in

Fig. 3 is shown which is calculated for $\tau = 0.06D$, $\alpha = 45°$, $\theta_0 = 15°$, $d = 100b$, and demonstrates the behavior typical for low-angle GBs [32]. More precisely, when φ increases, the energy first decreases, reaches its minimum at some equilibrium value φ_{eq} of the GB rotation angle, and then grows; see curve 1 in Fig. 3. In the case of high-angle GBs, D*W* can exhibit a more complicated behavior; see, for instance, curve 2 in Fig. 3. This curve is calculated at $\tau = 0.08D$, $\alpha = 45°$, $\theta_0 = 20°$, $d = 50b$. As it follows from curve 2, the dependence ΔW (φ) for a high-angle GB can have minimums additional to its main minimum. The additional minimums are associated with those of the dependence $\gamma_{GB}(\theta)$. Since the GB misorientation angle θ decreases during the GB rotation (see formula (A4) in Appendix), q may reach value corresponding to a minimum of the dependence $\gamma_{GB}(\theta)$. This dependence at the minimum dramatically changes its trend from a decreasing behavior to that showing an increase with rising θ. As a corollary, ΔW can have several additional minimums (at certain values of parameters characterizing the defect configuration) corresponding to metastable states of the rotating GB.

In next section, we will calculate and analyze the dependences of the equilibrium GB rotation angle φ_{eq} on applied stress and various geometric characteristics of the defect system under examination. In doing so, in the case of a configuration having several metastable states, we will consider the state with the minimum φ_{eq}, that is, the metastable state nearest to the initial one. In other words, in the case under discussion, we will exploit the zero temperature approximation with transitions between metastable states being forbidden.

4. DEPENDENCES OF EQUILIBRIUM ANGLE φ_{eq} OF GRAIN BOUNDARY ROTATION ON APPLIED STRESS AND GEOMETRIC CHARACTERISTICS OF THE DEFECT SYSTEM IN NANOCRYSTALLINE SOLIDS

As it follows from our previous examination, the key characteristic of a stress-driven GB rotation process is the equilibrium rotation angle φ_{eq}. In this context, for description of the stress-driven GB rotation process in a deformed nanocrystalline solid, it is highly important to calculate and analyze the dependences of the equilibrium GB rotation angle φ_{eq} on applied stress and various geometric characteristics of the defect system. Such calculations and analysis represent the main subject of this section.

Fig. 4 presents the dependences φ_{eq} on the applied shear stress τ, for various values of other parameters of the system. All the dependences are indicative of the logical trend that the angle φ_{eq} monotonously (in the near-linear way) grows with rising the applied stress. For values of parameters exploited in our calculations, typical values of the equilibrium GB rotation angle φ_{eq} are in the range from several degrees to ~15°. As to more details, curves in Fig. 4a are calculated for $\theta_0 = 15°$, $\alpha = 45°$ as well as values of $d = 25b$, $50b$, $100b$, and $200b$. From Fig. 4a it follows that rotations of short GBs are enhanced compared to those of long GBs. This trend is due to the screening effect of the free surface on the stress field of the disclination whose strain energy (given by formula (A1) in Appendix) depends on d as $\propto d^2$. (For shorter GBs, the triple junction A is evidently located closer to the free surface, than for longer GBs).

Curves $\varphi_{eq}(\tau)$ in Fig. 4b are calculated for $\alpha = 45°$, $d = 100b$ as well as values of $\theta_0 = 15°$, 32°, 38.21° and 60°. These values of the GB misorientation angle are taken, for the following reasons. Value of 15° is the minimum limit for angles characterizing high-angle GBs (and, at the same time, the maximum limit for angles characterizing low-angle GBs). Values of 32° and 38.21° are close to each other, but they correspond to principally different cases. So, GB with $\theta_0 = 32°$ has the maximum value of the GB energy density near the edge of a cusp inherent to the dependence $\gamma_{GB}(\theta)$, whereas the misorientation angle 38.21° specifies a minimum (corresponding to GB with $\Sigma 7$) of the dependence $\gamma_{GB}(\theta)$. Therefore, during the GB rotation and associated decrease in the GB misorientation angle, the GB energy density decreases and increases for $\theta_0 = 32°$ and 38.21°, respectively. Value of 60° is treated as the limiting case unfavorable for GB rotation, because of both large misorientation angle θ_0 and minimum of the GB energy density γ_{GB}. In general, from Fig. 4b it is well seen the trend that the GB rotation is hampered when the misorientation angle θ_0 increases (due to the contribution to ΔW from the disclination energy given by formula (A1) in Appendix).

Curves $\varphi_{eq}(\tau)$ in Fig. 4c are calculated for $\theta_0 = 15°$, $d = 100b$ as well as values of $\alpha = 15°$, 30°, 45°, 60°, and 75°. As it follows from Fig. 4c, the angle α influences the GB rotation process in a

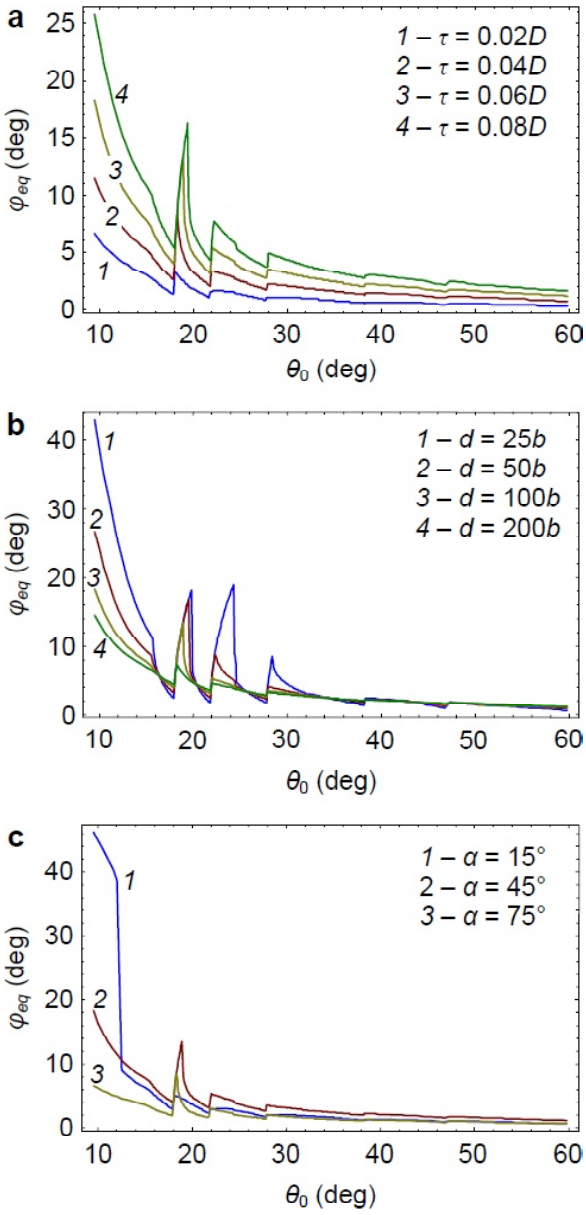

Fig. 5. (Color online) Dependences of the equilibrium rotation angle φ_{eq} on the misorientation angle θ_0 at (a) $d = 100b$, $\alpha = 45°$, and $\tau = 0.02D$, $0.04D$, $0.06D$, $0.08D$ (curves *1*, *2*, *3*, *4*, respectively); (b) $\tau = 0.06D$, $\alpha = 45°$, and $d = 25b$, $50b$, $100b$, $200b$ (curves *1*, *2*, *3*, *4*, respectively); (c) $\tau = 0.06D$, $d = 100b$, and $\alpha = 25°$, $45°$, $75°$ (curves *1*, *2*, *3*, respectively).

complicated manner which is not completely illustrated by this Figure. The influence in question becomes more evident from curves $\varphi_{eq}(\alpha)$ (see Fig. 7 and its discussion presented below). Nevertheless, even Fig. 4c shows that rotations of GBs oriented near perpendicular to the free surface are more hampered then those of GBs with other orientations of their planes (see curve 5).

Fig. 5 presents the dependences of φ_{eq} on the initial misorientation angle θ_0 of the rotating GB, for various values of other parameters of the defect system under consideration. The general trend is evident which is decrease in the equilibrium GB rotation angle φ_{eq} with increase in θ_0. However, in the areas where the GB misorientation angle is close to those of special GBs, there are "bursts" especially pronounced for special GBs with lowest misorientation angles (GBs with $\Sigma 31$, $\Sigma 21$, and $\Sigma 13$; see Fig. A2 in Appendix).

Curves $\varphi_{eq}(\theta_0)$ in Fig. 5a are calculated for $d = 100b$, $\alpha = 45°$ as well as values of the shear stress $\tau = 0.02D$, $0.04D$, $0.06D$ and $0.08D$, where $D = G/[2\pi(1 - \nu)]$, G is the shear modulus, and ν is the Poisson ratio. Larger values of τ correspond to larger values of φ_{eq}. "Bursts" for special GBs with misorientation angles >30° are insignificant, because the contribution of the GB energy density to ΔW is small compared to that from the disclination energy.

Curves $\varphi_{eq}(\theta_0)$ in Fig. 5b are calculated for $\tau = 0.06D$, $\alpha = 45°$ as well as values of $d = 25b$, $50b$, $100b$, and $200b$. From these curves it is interesting to note that the dependences $\varphi_{eq}(\theta_0)$ exhibit anomalous behavior in those narrow intervals of the misorientation angle θ_0, that precede "bursts". More precisely, the GB rotation angle is larger for longer GBs in these narrow intervals. The reason for the anomalous behavior is the fact that these narrow intervals correspond to decreasing segments of the GB energy density function $\gamma_{GB}(\theta)$ (see Fig. A2 in Appendix), in which case the energy density γ_{GB} grows, instead of decreasing, with rising rotation angle φ.

Curves $\varphi_{eq}(\theta_0)$ in Fig. 5c are calculated for $\tau = 0.06D$, $d = 100b$ as well as values of $\alpha = 15°$, $45°$, and $75°$. In general, this Figure as well as Figs. 5a and 5b are indicative of the fact that, for high-angle GBs specified by misorientation angles >30°, typical rotation angles $\varphi_{eq} < 5°$; for high-angle GBs with misorientation angles being in the range 15–30°, the rotation angles $\varphi_{eq} < 20°$; whereas low-angle GBs with misorientation angles <15°, can be rotated by large angles $\varphi_{eq} \geq 40°$.

Fig. 6 shows the dependences of φ_{eq} on the characteristic distance d between the triple junction A and the free surface (Fig. 1), for various values of other parameters specifying the defect system under our consideration. Curves $\varphi_{eq}(d)$ in Fig. 6a are calculated for $\theta_0 = 15°$, $\alpha = 45°$ as well as values of $\tau = 0.02D$, $0.04D$, $0.06D$, and $0.08D$. Curves $\varphi_{eq}(d)$ in Fig. 6b correspond to $\tau = 0.06D$, $\alpha = 45°$, and $\theta_0 = 15°$, $32°$, $38.21°$, and $60°$. Curves $\varphi_{eq}(d)$ in Fig. 6c are calculated for $\tau = 0.06D$, $\theta_0 = 15°$ as well as $\alpha = 15°$, $30°$, $45°$, $60°$, and $75°$. In most cases, the dependences $\varphi_{eq}(d)$ are monotonously

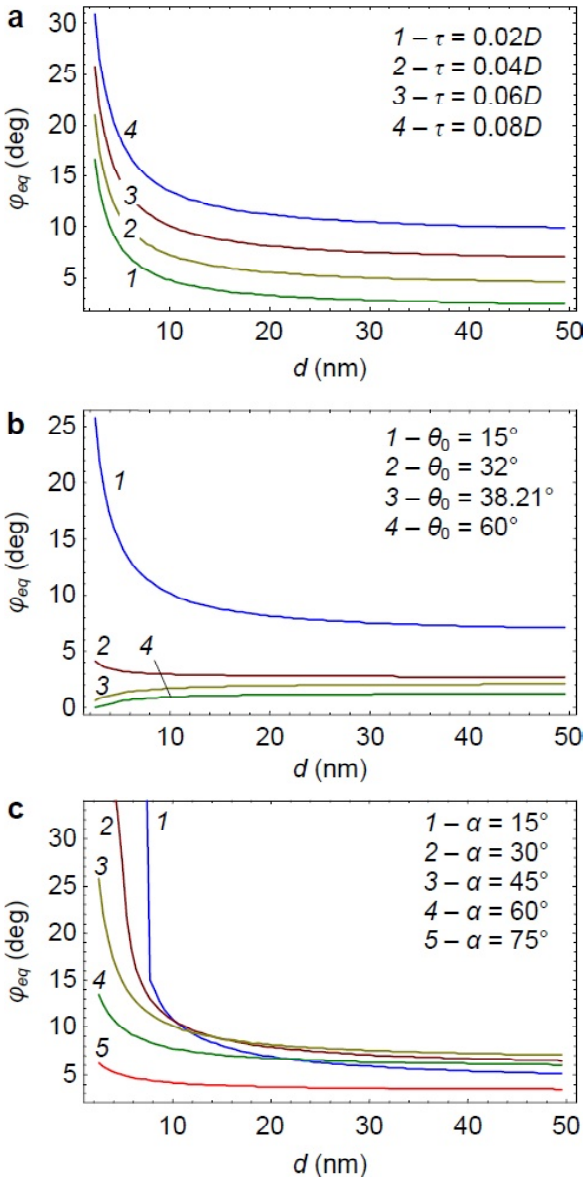

Fig. 6. (Color online) Dependences of the equilibrium rotation angle φ_{eq} on the parameter d (the distance between the triple junction A and the free surface) at (a) $\theta_0 = 15°$, $\alpha = 45°$, and $\tau = 0.02D$, $0.04D$, $0.06D$, $0.08D$ (curves *1*, *2*, *3*, *4*, respectively); (b) $\tau = 0.06D$, $\alpha = 45°$, and $\theta_0 = 15°$, 32°, 38.21°, 60° (curves *1*, *2*, *3*, *4*, respectively); (c) $\tau = 0.06D$, $\theta_0 = 15°$, and $\alpha = 15°$, 30°, 45°, 60°, 75° (curves *1*, *2*, *3*, *4*, *5*, respectively).

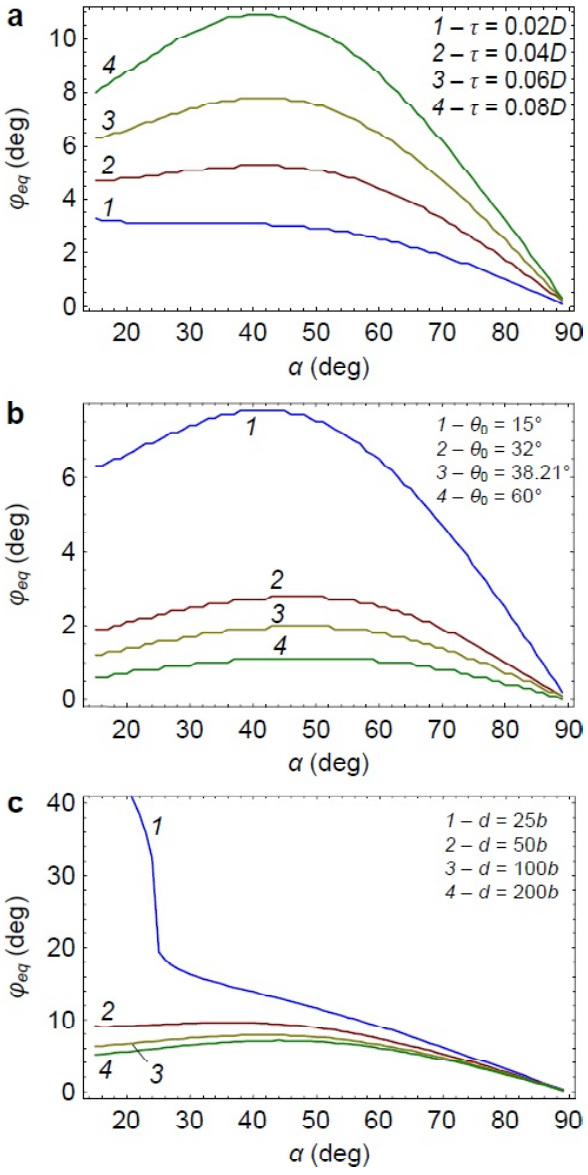

Fig. 7. (Color online) Dependences of the equilibrium rotation angle φ_{eq} on the angle a at (a) $d = 100b$, $\theta_0 = 15°$, and $\tau = 0.02D$, $0.04D$, $0.06D$, $0.08D$ (curves *1*, *2*, *3*, *4*, respectively); (b) $\tau = 0.06D$, $d = 100b$, and $\theta_0 = 15°$, 32°, 38.21°, 60° (curves *1*, *2*, *3*, *4*, respectively); (c) $\tau = 0.06D$, $\theta_0 = 15°$, and $d = 25b$, $50b$, $100b$, $200b$ (curves *1*, *2*, *3*, *4*, respectively).

decreasing functions of d, except for the situations where the rotating GBs in their initial states are special ones; see curves 3 and 4 in Fig. 6b, corresponding to the GB misorientation angles 38.21° and 60°, respectively. It is seen that these curves are monotonously growing functions of d, in contrast to other curves presented in Fig. 6. The reasons for the specific character of the curves 3 and 4 were discussed above as those related to non-monotonous behavior of the GB energy density γ_{GB} during the GB rotation process. Also, with curves presented in Fig. 6c, we conclude that GB rotations are enhanced, and the equilibrium rotation angle φ_{eq} increases, if the distance between the triple junction A and the free surface decreases. Say, for d<10 nm, the angle φ_{eq} reaches values of around 30° or more.

Fig. 7 presents the dependences of φ_{eq} on the angle α between the free surface and the rotating GB in its initial state (Fig. 1), for various values of

other parameters specifying the defect system under our consideration. Curves $\varphi_{eq}(\alpha)$ in Fig. 7a are calculated for $d = 100b$, $\theta_0 = 15°$ as well as $\tau = 0.02D$, $0.04D$, $0.06D$, and $0.08D$. Curves $\varphi_{eq}(\alpha)$ in Fig. 7b correspond to $\tau = 0.06D$, $d = 100b$ as well as $\theta_0 = 15°$, 32°, 38.21°, and 60°. Curves φ_{eq}(a) in Fig. 7c are calculated for $\tau = 0.06D$, $\theta_0 = 15°$ as well as $d = 25b$, $50b$, $100b$, and $200b$. From a general viewpoint, it is evident that the angle α influences the total energy change ΔW through the two factors. The first factor is the plastic deformation work (see formula (A8) in Appendix) in which the angle α specifies the orientation of GB dislocation glide/movement relative to the plane of the maximum shear stress action. With this factor, the optimum angle α enhancing the GB rotation process is the angle providing the same orientation of the planes under discussion (in our case, $\alpha = 45°$). The second factor is related to the fact that the total energy change ΔW is influenced by the angle a through sensitivity of the GB length $l = d/\sin(\alpha + \varphi)$ to α. When α diminishes, the GB length evidently decreases more rapidly during the GB rotation and thus leads to more profit in the total energy change ΔW. On the contrary, if the angle α is valued near 90°, the GB length very weakly changes during the GB rotation.

Competition of the two factors under our discussion is reflected in Fig. 7. In particular, as it follows from Fig. 7a, for comparatively large levels of the applied stress (see curves 2–4), each of the dependences φ_{eq}(a) has a well pronounced maximum at $\alpha \approx 40°$. At the same time, for smaller stress level (see, e.g., curve *1*), the contribution of the plastic deformation work to ΔW is small, and therefore the dependence $\varphi_{eq}(\alpha)$ monotonously decreases. In these circumstances, rotation of GBs making low angles with the free surface is enhanced despite their non-optimal orientation relative to the external shear stress.

The dependences presented in Fig. 7c have a character similar to that of curves shown in Fig. 7a. More precisely, for GB configurations with low values of d (see curve *1*), the dependence $\varphi_{eq}(\alpha)$ monotonously decreases, as with the case of low stresses. In doing so, however, the reason for the behavior in question is different from that in the case of low stresses. Actually, GBs characterized by low values of α in their initial states are by practice parallel with the free surface. In addition, since d is small, such GBs are located in the vicinity of the free surface. As a corollary, the stresses created by a rotating GB and its triple junction A with neighboring static GBs are effectively screened by the free surface, whereas the plastic deformation work is small due to small displacements of GB dislocations. These factors lead to the crucial contribution of the GB energy density to both DW and thereby the discussed character of the dependences $\varphi_{eq}(\alpha)$. For large values of d, each of the dependences $\varphi_{eq}(\alpha)$ has its maximum whose position tends to be closer to 45° with rising d. Also, as it follows from Fig. 7, rotations of GBs having their planes near perpendicular to the free surface are by practice forbidden (with the proviso that the plane of the maximum shear stress action is oriented by 45° relative to the free surface).

5. CONCLUDING REMARKS

Thus, we theoretically examined stress-driven rotations of high-angle GBs near free surfaces (Fig. 1) in mechanically loaded nanocrystalline solids such as nanowires, micropillars, films and bulk materials with nanocrystalline structures. Within our approach, rotation of a high-angle GB was described as a process realized through cooperative, stress-driven displacements of GB dislocations continuously distributed along the GB and characterized by infinitesimally small Burgers vectors. In the exemplary case of Ni, it was demonstrated that the GB rotation process is energetically favorable in wide ranges of parameters characterizing the GB configuration and mechanical load of the nanocrystalline specimen containing the configuration. The key characteristic of a stress-driven GB rotation process was identified to be the equilibrium rotation angle φ_{eq} corresponding to a minimum of the system energy. In certain conditions, there are several metastable states (corresponding to several minimums of the energy) of a rotating GB near the specimen free surface.

For characterization of the stress-driven GB rotation process in a deformed nanocrystalline solid, we calculated and analyzed the dependences of the equilibrium GB rotation angle φ_{eq} on the applied stress τ and various geometric parameters of the defect system. These parameters are the tilt misorientation angle θ_0 of the rotating GB; the distance d between the triple junction A (serving as a rotation axis for the rotating GB) and the free surface; and the angle α made by the rotating GB plane and the free surface (Fig. 1). In our calculations, we revealed the following trends. The equilibrium GB rotation angle φ_{eq} monotonously (in the near-linear way) grows with rising the applied stress τ (Fig. 3). Also, φ_{eq} tends to decrease when θ_0 and/or d increases (Figs. 4 and 5). Besides, with rising α,

the equilibrium GB rotation angle φ_{eq} first increases, reaches its maximum at $\alpha \approx 45°$, and then decreases down to 0 when α approaches 90° (Fig. 6). However, in certain conditions, there are deviations from the aforesaid trends. In particular, special GBs characterized by low energies behave in the way different from the trends. Rotations of special GBs are enhanced, and the dependences $\varphi_{eq}(\theta_0)$ exhibit "bursts" corresponding to these special GBs (Fig. 5). Besides, for special GBs, the dependences $\varphi_{eq}(d)$ are increasing functions, in contrast to decreasing functions that characterize general GBs. In addition, we found that, for low values of τ and d, the dependence $\varphi_{eq}(\alpha)$ deviates from its standard version. More precisely, this dependence becomes monotonously decreasing function, in which case rotations of GBs making low angles with the free surface are enhanced.

Values of the GB rotation angle φ_{eq} in nanocrystalline Ni range rather widely from units to tens of degrees, depending on parameters of GB configuration (Figs. 4–7). This is well consistent with the experimental observation [30] of GB rotations in mechanically loaded nanocrystalline Ni nanopillars. Also, the suggested representations on a new physical mechanism/mode of plastic deformation occurring through stress-driven rotations of high-angle GBs in nanocrystalline solids are indirectly supported by the experimental observation [31] of intense GB deformation processes - in particular, GB sliding - in ultrafine-grained micropillars of Al-based alloy. In this case, the stress-driven GB rotations can provide accommodation of GB sliding and serve as a special (new) GB deformation mode itself.

In addition, stress-driven GB rotations can serve as accommodating processes for grain growth and crystal lattice rotations within isolated grains or their groups in deformed nanocrystalline solids. In particular, such grain growth and crystal lattice rotations were experimentally observed in regions near crack tips in nanocrystalline and ultrafine-grained materials [40–44]. In these areas, stresses are very high, and it is logical to assume that stress-driven GB rotations can occur.

ACKNOWLEDGEMENT

This work was supported by the Ministry of Education and Science of the Russian Federation (Grant 14.B25.31.0017 and Contract 8025), St. Petersburg State University research grant 6.37.671.2013, and Russian Foundation for Basic Research (Grants 12-01-00291-a and 12-01-31350).

APPENDIX

In this Appendix, we will calculate all the terms figuring on the right-hand side of formula (5). This will allow us to calculate the total energy change ΔW (see the main text).

The proper elastic energy W^{Δ} of the wedge disclination A located near the free surface [Fig. 1c] is given by the known formula [36]:

$$W^{\Delta} = \frac{D\omega^2 d^2}{2}, \qquad (A1)$$

where $D = G/[2\pi(1 - \nu)]$, G is the shear modulus, and ν is the Poisson ratio. The disclination strength ω, as it has been noted previously [32], is equal to the difference, $\omega = \theta - \theta_0$, between the GB misorientation angles after and before the GB rotation (θ and θ_0, respectively).

For our further calculations of the terms figuring on the right-hand side of formula (5), let us represent the misorientation angle θ of the GB in its final state as a function of the GB rotation angle j and the misorientation angle θ_0 of the GB in its initial state. By analogy with formula (1), the GB misorientation angle θ is in the following Frank relationship with the "perpendicular" component $B_{\perp} = B\cos\varphi$ (see Fig. 1c) of the sum Burgers vector of the GB located in its final position AB':

$$B_{\perp} = B\cos\varphi = 2l\tan(\theta/2). \qquad (A2)$$

Now let us consider those GB dislocations that "survived" after the GB rotation. (Other GB dislocations disappear at the free surface during the GB rotation.) For evident geometric reasons (see Fig. 1c), these GB dislocations occupy some finite segment of the GB when it is located in its initial position AB, and the segment in question has the length of $l\cos\varphi$. The sum Burgers vector of these GB dislocations is given as: $B = (l\cos\varphi/l_0)B_0$. With this relation, from formula (1) one obtains:

$$B = 2l\cos\varphi\tan(\theta_0/2). \qquad (A3)$$

From formulas (A2) and (A3) we find the following relationship between θ, φ, and θ_0:

$$\theta = 2\arctan\left(\cos^2\varphi\tan\frac{\theta_0}{2}\right). \qquad (A4)$$

This relationship is indicative, in particular, of the fact that the GB misorientation angle decreases during the GB rotation.

Now let us return to calculation of the terms figuring on the right-hand side of formula (5). The free

surface step formed during the GB rotation (Figs. 1b and 1c) consists of elementary steps each being formed by a GB dislocation during its enter/disappearance on the free surface. Each elementary step has the length equal to infinitesimally small Burgers vector magnitude of the disappeared GB dislocation. As a corollary, the energy W_{step} of the free surface step is proportional to the decrease, B-B_0, in the sum Burgers vector of the GB due its rotation. That is, $W_{step} = \gamma_s(B - B_0)$, with γ_s being the free surface energy density (per unit area). With this relation and formulas (1) and (A3), one obtains:

$$W_{step} = 2\gamma_s \tan\frac{\theta_0}{2}\left(l_0 - l\cos\varphi\right) = 2\gamma_s d \tan\frac{\theta_0}{2}\left[\frac{1}{\sin\alpha} - \frac{\cos\varphi}{\sin\left(\alpha+\varphi\right)}\right]. \tag{A5}$$

The plastic deformation work is calculated by integration of elemental works each being related to displacement of a GB dislocation with infinitesimal Burgers vector during the GB rotation. In this situation, we have:

$$A_{pl} = \tau\cos\left(\pi/2 - 2\alpha\right)\int_0^{l_0} s(r)\,\mathrm{d}B_0, \tag{A6}$$

where $\mathrm{d}B_0 = (B_0/l_0)\mathrm{d}r$ is the Burgers vector of GB dislocations located at an infinitesimally small GB fragment of length dr, r the distance between the GB fragment and the triple junction, and $s(r)$ is the displacement of the GB fragment during the GB rotation under the applied shear stress τ. In writing formula (A6), for definiteness, we assume that the plane of the maximum shear stress action makes the angle 45° with the free surface, and the angle between this plane and dislocation glide plane is equal to $\pi/4 - \alpha$. (The latter explains the presence of cos in the expression for A_{pl}). With geometry of the considered system (Fig. 1c), the dependence $s(r)$ is calculated as follows:

$$s(r) = \begin{cases} r\tan\varphi, & \text{if } 0 \le r \le l\cos\varphi, \\ \left(l_0 - r\right)\tan\alpha, & \text{if } l\cos\varphi \le r \le l_0. \end{cases} \tag{A7}$$

Substitution of (A7) to formula (A6) gives:

$$A_{pl} = \tau d^2 \tan\frac{\theta_0}{2}\,\frac{\sin\varphi\cos\left(\pi/2 - 2\alpha\right)}{\sin\alpha\sin\left(\alpha+\varphi\right)}. \tag{A8}$$

In order to calculate the energy W_p figuring on the right-hand side of formula (5), it is convenient to represent the dislocation structure of the GB AB' as a superposition of the two continuous distributions of edge dislocations with Burgers vectors perpendicular and parallel to the GB plane (see Fig. 2). The energy of the distribution of GB dislocations characterized by Burgers vectors perpendicular to the GB plane has been taken into consideration through its equivalent disclination model in the expression (A1). More precisely, following the theory of disclinations in solids [36], stress fields created by GB dislocations characterized by Burgers vectors perpendicular to the GB plane and located at the GB AB' are well described as those created by a wedge disclination located at the triple junction A. Therefore, the strain energy of such GB dislocation distribution is in a good approximation equal to the strain energy of the disclination.

Also, the distribution of GB dislocations characterized by Burgers vectors parallel to the GB plane (that is, the Burgers vectors with magnitudes $\mathrm{d}B_{\|} = (B_{\|}/l)\mathrm{d}r$) serves as a powerful source of long-range stresses. Its contribution to the strain energy of the GB can be calculated in the standard way [45] as the work spent to generation of the dislocations in their stress fields. To do so, we consider a GB fragment of infinitesimally small length dr (Fig. A1). This fragment is characterized by infinitesimally small Burgers vector magnitude $dB_{\|} = (B_{\|}/l)dr$ and in some approximation can be viewed as a GB dislocation with this Burgers vector magnitude. Let us calculate the work spent to introduce such a dislocation from the free surface to its final position in the stress field created by the continuous dislocation distribution under our examination. (The path of the dislocation introduction is indicated by arrow in Fig. A1). As a result, we find the (infinitesimally small) energy dW_p of this GB fragment as follows:

$$\mathrm{d}W_p(r) = -\frac{B_{\|}\,\mathrm{d}r}{2l}\int_0^{r\sin\left(\alpha+\varphi\right)}\left[\sin\left(\alpha+\varphi\right)\sigma_{xy}\left(x, r\cos\left(\alpha+\varphi\right)\right) + \cos\left(\alpha+\varphi\right)\sigma_{yy}\left(x, r\cos\left(\alpha+\varphi\right)\right)\right]\mathrm{d}r. \tag{A9}$$

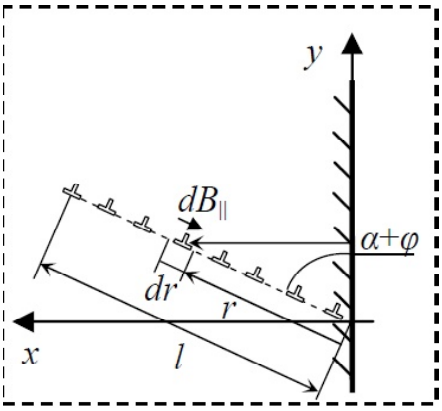

Fig. A1. Continuous distribution of edge dislocations having infinitesimally small Burgers vectors is located near the specimen free surface.

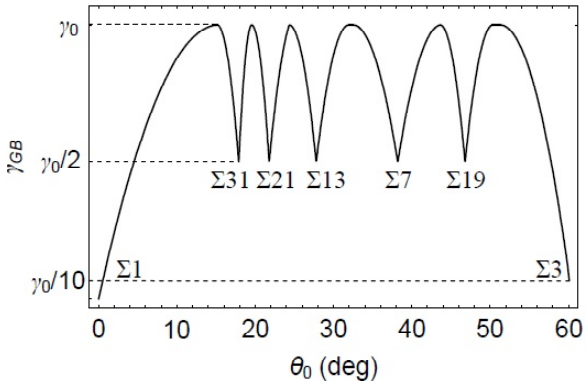

Fig. A2. Idealized dependence of the grain boundary energy density γ_{GB} on tilt misorientation angle q, for high-angle tilt boundary of <111> type in nickel (in spirit of the approach [34]).

Here σ_{xy} and σ_{yy} are the stress tensor components created by the continuously distributed dislocations near the free surface, and the parameter r specifies the spatial location of the GB fragment (the distance between the fragment and the triple junction A) and varies from 0 to l.

The stresses, σ_{xy} and σ_{yy} can be calculated by integration of the known expressions [46] for the stress fields, $\sigma_{xy}^{(1)}$ and $\sigma_{yy}^{(1)}$, respectively, of a sole edge dislocation near the free surface. The latter stress fields in the coordinate system shown in Fig. A1 are given as:

$$\sigma_{xy}^{(1)}(x,y)/D = b_x\left[-\frac{x_-}{r_-^2}+\frac{2x^3}{r_-^4}+\frac{x_-}{r_+^2}+\frac{2x_+\left(x'^2+6x'x-x^2\right)}{r_+^4}-\frac{16xx'x_+^3}{r_+^6}\right]+$$
$$b_y\left[-\frac{y_-}{r_-^2}+\frac{2y_-x_-^2}{r_-^4}+\frac{y_-}{r_+^2}-\frac{2y_-\left(x'^2+4x'x+x^2\right)}{r_+^4}+\frac{16y_-xx'x_+^2}{r_+^6}\right], \quad \text{(A10)}$$

$$\sigma_{yy}^{(1)}(x,y)/D = b_x\left[-\frac{y_-}{r_-^2}+\frac{2y_-x_-^2}{r_-^4}+\frac{y_-}{r_+^2}+\frac{2y_-\left(2x'^2+4x'x-x^2\right)}{r_+^4}-\frac{16y_-xx'x_+^2}{r_+^6}\right]+$$
$$b_y\left[\frac{3x_-}{r_-^2}-\frac{2x_-^3}{r_-^4}-\frac{3x+5x'}{r_+^2}+\frac{2x_+\left(3x'^2+10x'x+x^2\right)}{r_+^4}-\frac{16xx'x_+^3}{r_+^6}\right], \quad \text{(A11)}$$

where $x_\pm = x \pm x'$, $y_- = y - y'$, $r_\pm = \sqrt{x_\pm^2 + y_-^2}$, x' and y' are the coordinates of the sole dislocation, b_x and b_y are the projections of the dislocation Burgers vector on the coordinate axes Ox and Oy, respectively. In our case (Fig. A1), all the dislocation cores lie on one line, and therefore their coordinates can be effectively expressed through the parameter r and the angle $\alpha + \varphi$ as follows: $x' = r\sin(\alpha + \varphi)$, $y' = r\cos(\alpha + \varphi)$. The Burgers vector projections are evidently given as: $b_x = dB_{||}\sin(\alpha + \varphi)$, and $b_y = dB_{||}\cos(\alpha + \varphi)$. With these expressions substituted to formulas (A10) and (A11), we find the stress tensor components σ_{xy} and σ_{yy} as the following integrals (for details, see, e.g., [47]):

$$\sigma_{xy}(x,y) = \int_0^l \rho\sigma_{xy}^{(1)}\left(x,y;x' = r\sin(\alpha+\varphi), y' = r\sin(\alpha+\varphi)\right)dr, \quad \text{(A12)}$$

$$\sigma_{yy}(x,y) = \int_0^l \rho\sigma_{y}^{(1)}\left(x,y;x' = r\sin(\alpha+\varphi), y' = r\sin(\alpha+\varphi)\right)dr, \quad \text{(A13)}$$

Here $\rho = B_{||}/(l dB_{||})$ denotes the linear density of the dislocations in their continuous distribution.

The expressions (A10)–(A13) allow us to calculate the integral (A9). In its turn, the total energy is calculated by integrating the expression (A9), that is:

$$W_p = \int_0^l \mathrm{d}W_p(r). \qquad \text{(A14)}$$

Integral (A14), in general, can be calculated analytically. However, the analytical approach is labor-consuming, and its presentation in paper needs too much space. Therefore, in our examination, the energy W_p was numerically calculated with the aid of formulas (A9)–(A14).

The GB energy density $\gamma_{GB}(\theta)$ (figuring on the right-hand side of formula (5)), as it is well-known [34], depends on the GB misorientation angle. In most materials the GB energy γ_{GB} versus tilt misorientation θ, for $\theta > 15°$, is a slowly increasing or approximately constant function of θ with energy "cusps" associated with special GBs in some narrow intervals of θ [34]. Figure A2 shows such an idealized dependence $\gamma_{GB}(\theta)$ taken from paper [48] in the case of tilt boundary of <111> type in Ni. This dependence reflects the previously noted specific features, that is, an approximately constant level (shown as γ_0) of the energy in wide intervals of θ with energy "cusps" associated with special GBs in some narrow intervals of θ. For definiteness, the minimum values of the energy are taken as $\gamma_0/2$, except for the special GB with the misorientation angle 60° (and $\Sigma 3$), whose energy is taken as $\gamma_0/10$.

REFERENCES

[1] L. Lu, M.L. Sui and K. Lu // *Science* **287** (2000) 1463.

[2] I.A. Ovid'ko // *Science* **295** (2002) 2386.

[3] M. Chen, E. Ma, K.J. Hemker, H. Sheng, Y.M. Wang and X. Cheng // *Science* **300** (2003) 1275.

[4] M.D. Uchic, D.M. Dimiduk, J.N. Florando and W.D. Nix // *Science* **305** (2004) 986.

[5] J.R. Greer and W.D. Nix // *Phys. Rev. B* **73** (2006) 245410.

[6] X.L. Wu and Y.T. Zhu // *Phys. Rev. Lett.* **101** (2008) 025503.

[7] X.L. Wu, Y.T. Zhu, Y.G. Wei and Q. Wei // *Phys. Rev. Lett.* **103** (2009) 205504.

[8] S.V. Bobylev and I.A. Ovid'ko // *Phys. Rev. Lett.* **103** (2009) 135501;

[9] Q. Yu, Z.-W. Shan, J. Li, X. Huang, L. Xiao, J. Sun and E. Ma // *Nature* **463** (2010) 335. S.V. Bobylev and I.A. Ovid'ko // *Phys. Rev. B* **84** (2011) 054111.

[10] S.V. Bobylev, N.F. Morozov and I.A. Ovid'ko // *Phys. Rev. Lett.* **105** (2010) 055504; S.V. Bobylev, N.F. Morozov and I.A. Ovid'ko // *Phys. Rev. B* **84** (2011) 094103.

[11] Y.M. Wang, R.T. Ott, A.V. Hamza, M.F. Besser, J. Almer and M.J. Kramer // *Phys. Rev. Lett.* **105** (2010) 215502.

[12] I.A. Ovid'ko and A.G. Sheinerman // *Rev. Adv. Mater. Sci*. **27** (2011) 189.

[13] I.A. Ovid'ko // *Appl. Phys. Lett.* **99** (2011) 0619071.

[14] I.A. Ovid'ko and A.G. Sheinerman // *Rev. Adv. Mater. Sci*. **29** (2011) 105.

[15] I.A. Ovid'ko and T.G. Langdon // *Rev. Adv. Mater. Sci*. **30** (2012) 103.

[16] A. Sedlmayr, E. Bitzek, D.S. Gianola, G. Richter, R. Mönig and O. Kraft // *Acta Mater.* **60** (2012) 3985.

[17] C. Chisholm, H. Bei, M.B. Lowry, J. Oh, S.A. Syed Asif, O.L. Warren, Z.W. Shan, E.P. George and A.M. Minor // *Acta Mater*. **60** (2012) 2258.

[18] Y. Zhu, Q. Qin, F. Xu, F. Fan, Y. Ding, T. Zhang, B.J. Wiley and Z.L. Wang // *Phys. Rev. B* **85** (2012) 045443.

[19] T. Mandal, P.K. Maiti and C. Dasgupta // *Phys Rev B* **86** (2012) 024101.

[20] I.A. Ovid'ko // *Scr. Mater.* **66** (2012) 402.

[21] R.G. Chembarisova, M.I. Latypov and I.V. Alexandrov // *Rev. Adv. Mater. Sci* **31** (2012) 100.

[22] O. Sitdikov, S. Krymskiy, M. Markushev, E. Avtokratova and T. Sakai // *Rev. Adv. Mater. Sci*. **31** (2012) 62.

[23] I.A. Ovid'ko and A.G. Sheinerman // *Rev. Adv. Mater. Sci*. **32** (2012) 61.

[24] N.F. Morozov, I.A. Ovid'ko, A.G. Sheinerman and N.V. Skiba // *Rev. Adv. Mater. Sci* **32** (2012) 75.

[25] G. Liu, G.J. Zhang, F. Jiang, X.D. Ding, Y.J. Sun and E. Ma // *Nature Mater*. **12** (2013) 344.

[26] A.T. Jennings, C.R. Weinberger, S.-W. Lee, Z.H. Aitken, L. Meza and J.R. Greer // *Acta Mater*. **61** (2013) 2244.

[27] K. Zhou, A.A. Nazarov and M.S. Wu // *Phys. Rev. B* **73** (2006)045410; K. Zhou, A.A. Nazarov and M.S. Wu // *Phys. Rev. Lett.* **98** (2007) 035501.

[28] K. Zhou, M.S. Wu and A.A. Nazarov // *Acta Mater*. **56** (2008) 5828.

[29] Z.X. Wu, Y.W. Zhang, M.H. Jhon, J.R. Greer and D.J. Srolovitz // *Acta Mater*. **61** (2013) 1831.

[30] Z.X. Wu, Y.W. Zhang, M.H. Jhon and D.J. Srolovitz // *Acta Mater*. **61** (2013) 5807.
[31] D. Jang and J.R. Greer // *Scr. Mater.* **64** (2011) 77.
[32] N.Q. Chinh, T. Gyori, R.Z. Valiev, P. Szommer, G. Varga, K. Havancsak and T.G. Langdon // *MRS Commun*. **2** (2012) 75.
[33] S.V. Bobylev and I.A. Ovid'ko // *Phys. Rev. Lett.* **109** (2012) 175501.
[34] C.C. Koch, I.A. Ovid'ko, S. Seal and S. Veprek, *Structural nanocrystalline materials: Fundamentals and applications* (Cambridge University Press, Cambridge, 2007).
[35] A.P. Sutton and R.W. Balluffi, *Interfaces in crystalline materials* (Oxford Science Publications, Oxford, 1996).
[36] T.G. Langdon // *J. Mater. Sci.* **41** (2006) 597.
[37] A.E. Romanov and V.I. Vladimirov, In: *Dislocations in solids*, *vol. 9*, ed. by F.R.N. Nabarro (North Holland, Amsterdam, 1992), p. 191.
[38] M. Kleman and J. Friedel // *Rev. Mod. Phys.* **80** (2008) 61.
[39] A.E. Romanov and A.L. Kolesnikova // *Progr. Mater. Sci.* **54** (2009) 740.
[40] J.P. Hirth and J. Lothe, *Theory of Dislocations* (Wiley, New York, 1982).
[41] M. Ke, W.W. Milligan, S.A. Hackney, J.E. Carsley and E.C. Aifantis // *Nanostruct. Mater*. **5** (1995) 689.
[42] S. Cheng, Y. Zhao, Y. Wang, Y. Li, X.-L. Wang, P.K. Liaw and E.J. Lavernia // *Phys. Rev. Lett.* **104** (2010) 255501.
[43] Z. Shan, J.A. Knapp, D.M. Follstaedt, E.A. Stach, J.M.K. Wiezorek and S.X. Mao // *Phys. Rev. Lett.* **100** (2008) 105502.
[44] P. Liu, S.C. Mao, L.H. Wang, X.D. Han and Z. Zhang // *Scr. Mater.* **64** (2011) 343.
[45] S. Cheng, S.Y. Lee, L. Li, C. Lei, J. Almer, X.-L. Wang, T. Ungar, Y. Wang and P.K. Liaw // *Phys. Rev. Lett.* **110** (2013) 135501.
[46] T. Mura, In: *Advances in material research, vol. 3*, ed. by H. Herman (Interscience, New York, 1968), pp. 1–108.
[47] T.Mura, *Micromechanics of defects in solids* (Martinus Nijhoff Publishers, Dordrecht, 1987).
[48] S.V. Bobylev, M.Yu. Gutkin and I.A. Ovid'ko // *J. Phys.: Condens. Matter.* **15** (2003) 7925.
[49] K.E. Harris, V.V. Singh and A.H. King // *Acta Mater*. **46** (1998) 2623.